Applied Geochemistry 87 (2017) 108–121

Contents lists available at ScienceDirect

Applied Geochemistry

journal homepage: www.elsevier.com/locate/apgeochem

Kinetics of inorganic nitrogen turnover in a sandy seepage face on a subterranean estuary

J. Severino P. Ibánhez*, Carlos Rocha

Biogeochemistry Research Group, School of Natural Sciences, Geography Department, Trinity College, Dublin 2, Ireland

ARTICLE INFO

Editorial handling by Prof. M. Kersten.

Keywords:
SGD
Seepage face
Nitrate reduction
Aerobic nitrate reduction
DNRA
Ria Formosa

ABSTRACT

Subterranean estuary seepage faces are recognized as important reactive interfaces that regulate solute transport to coastal ecosystems via Submarine Groundwater Discharge (SGD). Here we describe benthic processes and rates driving the biogeochemical regulation of SGD-borne inorganic N loading into the Ria Formosa lagoon (Iberian peninsula) through a sandy seepage face. Maximum potential NO_3^- reduction rates, obtained by kinetic modeling of advection-controlled flow-through reactor experiments, ranged from 2.33 ± 1.06 to 14.17 ± 0.22 nmol cm^{-3} "bulk" sediment (bs) h^{-1}. Maximum potential nitrification ranged from 0 to 7.5 ± 1.3 nmol cm^{-3} bs h^{-1} while potential ammonium assimilation was valued at 2.0 ± 0.3 nmol cm^{-3} bs h^{-1}. These NO_3^- reduction rates are in good agreement with previous estimates obtained by diagenetic modeling of in-situ porewater NO_3^- vertical profiles at the same location. Potential NO_3^- reduction rates were very sensitive to temperature (Q_{10} = 3.5 ± 0.2). Porewater velocity seems to control net NO_3^- reduction rates, probably by determining solute distribution but also its supply to the microbial community by shaping the diffusive boundary layer around sediment particles. Nevertheless, NO_3^- reduction rates seem ultimately limited by organic matter availability at high velocities. Half-saturation constants of NO_3^- for NO_3^- reduction were low, suggesting that the NO_3^- reducing microbial community had high affinity for NO_3^-. In addition, our experiments provide evidence for the occurrence of alternative NO_3^- reduction pathways, including Dissimilatory Nitrate Reduction to Ammonium (DNRA) and apparent aerobic NO_3^- reduction within the shallow subsurface sediment layer (2–12 cm depth).

1. Introduction

Submarine Groundwater Discharge (SGD, *sensu* Burnett et al., 2003) is now recognized as a globally important transport vector of freshwater and solutes to the coastal zone (e.g., Moore, 2010; Kwon et al., 2014). Due to the inefficient use of fertilizers and ensuing widespread NO_3^- pollution of coastal aquifers observed worldwide, SGD has been putatively linked to the decline in water quality and trophic status of several coastal ecosystems (Hwang et al., 2005; Moore, 2010; Rocha et al., 2015). SGD is increasingly recognized as a relevant transport vector of nutrients to coastal systems and considered in current biogeochemical budget studies (e.g. Swaney and Giordani, 2011). Nevertheless, the direct quantification of Dissolved Inorganic Nitrogen (DIN) transport to the coastal zone by application of simplified mass balances, in which the non-conservative nature of DIN is ignored, to coastal aquifer systems may result in flawed predictions of N transport to surface waters. This is due to the active biogeochemical processing of DIN that occurs in the subterranean estuary (Bowen et al., 2007; Kroeger and Charette, 2008; Rocha et al., 2009), the subsurface mixing zone between groundwater and seawater (Moore, 1999). Available estimates of NO_3^- reduction rates occurring in subterranean estuaries are high, and occasionally drive significant reduction of SGD-borne NO_3^- fluxes to the coastal zone (Kroeger and Charette, 2008; Erler et al., 2014). However, there is also evidence that the magnitude of attenuation of NO_3^- loading through the seepage face, assumed to be mainly the result of heterotrophic denitrification, may be limited since other NO_3^- reducing pathways might coexist (Rocha et al., 2009; Sáenz et al., 2012; Ibánhez et al., 2013).

Although the autotrophic Anaerobic Ammonium Oxidation (anammox) process has been specifically shown to occur in subterranean estuaries (Kroeger and Charette, 2008; Sáenz et al., 2012), the occurrence of Dissimilatory Nitrate Reduction to Ammonium (DNRA) has only been inferred by mass balance and stoichiometric approaches (Bowen et al., 2007; Rocha et al., 2009; Ibánhez et al., 2013). These two processes, together with heterotrophic denitrification, are considered the main NO_3^- reducing pathways in the biosphere (although

* Corresponding author.
E-mail addresses: pinoibaj@tcd.ie (J.S.P. Ibánhez), rochac@tcd.ie (C. Rocha).

http://dx.doi.org/10.1016/j.apgeochem.2017.10.015
Received 31 July 2017; Received in revised form 17 October 2017; Accepted 19 October 2017
Available online 21 October 2017

Nomenclature

$R_{max}^{NO_3^-}$	Maximum NO_3^- reduction rate
$K_m^{NO_3^-}$	Half-saturation NO_3^- reduction constant
$R_{max}^{NO_2^-}$	Maximum NO_2^- reduction rate
$K_m^{NO_2^-}$	Half-saturation NO_2^- reduction constant
$R_{DNRA}^{NO_2^-}$	Maximum NO_2^- reduction to NH_4^+
$K_{DNRA}^{NO_2^-}$	Half-saturation NO_2^- reduction to NH_4^+ constant
$R_{ox}^{NH_4^+}$	NH_4^+ oxidation rate
R_{ads}	Kinetics rate of first order NH_4^+ adsorption-desorption
NH_{4eq}^+	Total NH_4^+ adsorbed at equilibrium in the reactor
NH_{4ads}^+	Total NH_4^+ adsorbed in the reactor
K_{decay}	Hyperbolic decay inhibition factor
$f_{inhibition}$	Inhibition factor
I_{nh}	Hyperbolic decay inhibition property
R_{assim}	NH_4^+ assimilation rate

anammox requires the prior reduction of NO_3^- to NO_2^-) (Thamdrup, 2012; Kraft et al., 2014). While anammox and heterotrophic denitrification act as sinks of bioavailable DIN, DNRA reduces NO_3^- to NH_4^+, thus recycling N into bioavailable forms and extending its residence time in the biosphere. Organic C and NO_3^- loading, together with temperature, seem to be the main factors determining the relative significance of these three processes (Kraft et al., 2014; Hardison et al., 2015). Thus, the ratio between organic C and NO_3^- availability might yet drive sequential shifting between these processes, with anammox favored at the lowest organic C to NO_3^- ratios, denitrification at intermediate ratios and DNRA at the highest (Algar and Vallino, 2014).

Due to the commonly low organic carbon concentrations found in permeable sediments, DNRA would at first glance be expected to play a minor role in processing NO_3^- loads in transit through subterranean estuaries (Santoro, 2009). However, the role of porewater advection in regulating substrate availability and driving reaction rates is not well resolved in these systems, and could indeed be determinant in our understanding of the biogeochemical role of seepage faces in modulating solute transport across the land-ocean boundary (Rocha, 2008). For example, on an annual basis, we have observed periods when SGD-borne NO_3^- fluxes at a seepage face increased at this site, in spite of significant in-situ NO_3^- reduction rates (Ibánhez et al., 2013), while the occurrence of DNRA could be inferred from mass balance and stoichiometric approaches (Rocha et al., 2009). The combination of DNRA with benthic organic matter remineralization would thus explain the apparent benthic enhancement of SGD-derived NO_3^- fluxes in the presence of significant NO_3^- reduction rates at the seepage face. This indicates that the ultimate role of the seepage face in subterranean estuaries in modulating benthic NO_3^- fluxes to surface waters is complex and locally variable in time and space.

Here, benthic reactivity affecting the DIN concentrations brought by inflowing groundwater was studied at a Ria Formosa (Southwestern Iberia) SGD seepage face. Flow-through reactor (FTR) experiments were complemented by mass balance and kinetic modeling of the resultant temporal dynamics of DIN compounds and used in combination to a) evaluate benthic biogeochemical processes involved in the modulation of NO_3^--rich SGD fluxes and b) to constrain the influence of environmental parameters on benthic reactivity.

2. Materials and methods

2.1. Study site and sampling strategy

The sampling site is located in the lower intertidal zone of the landward side of the Ancão peninsula (37°00′04″ N, 7°88′57″ W; Fig. 1), one of two sandy spits bounding the Ria Formosa coastal lagoon and within an area affected by nitrate-rich SGD (Leote et al., 2008; Rocha et al., 2009). NO_3^- and NH_4^+ content of up to 187 μM and 40 μM respectively were measured in the water seeping at the sampling site, with salinities as low as 16.8 (Leote et al., 2008). Sediment at the sampling site is composed mainly by medium-coarse sand (0.5 mm average grain size) with high hydraulic conductivity (1×10^{-3} cm s^{-1} in the top 20 cm; Rocha et al., 2009). Low standing stocks of particulate organic matter and low intermonth variability (< 0.8%; Ibánhez and Rocha, 2014a) characterized the sampled sediment during this study (October 2010 and January 2011).

A definition of the apparent vertical biogeochemical zonation present between 0 and 20 cm depth at the studied seepage face was achieved by diagenetic modeling of in situ NO_3^- porewater profiles from 0 to 20 cm depth (Ibánhez et al., 2013). Net NO_3^- production appeared restricted to the top 1–2 cm of the sediment column, while NO_3^- reduction was the dominant process in the underlying sediment layers down to 20 cm depth. Some of the in-situ porewater NO_3^- profiles also showed an apparent limitation of NO_3^- reduction with depth, particularly during the warmer months (Ibánhez et al., 2011, 2013). In these cases, the inclusion of a non-reactive sediment layer in depth in the diagenetic models significantly improved model fit of the data, and suggested that active NO_3^- reduction would be restricted to the top 12–15 cm deep sediment layer. On this basis and for this study, the sediment depth of interest was defined as the layer between 2 and 12 cm below the surface. Porosity measured in dedicated sediment cores taken from the site in October 2010 and January 2011 (Ibánhez and Rocha, 2014a) showed vertical uniformity at this depth (2–12 cm), with values approximating 0.3.

2.2. Sediment FTR experiments

A series of FTR experiments (experiments 2 and 9) were conducted in October 2010 and January 2011 (experiments 1 to 8). A complete

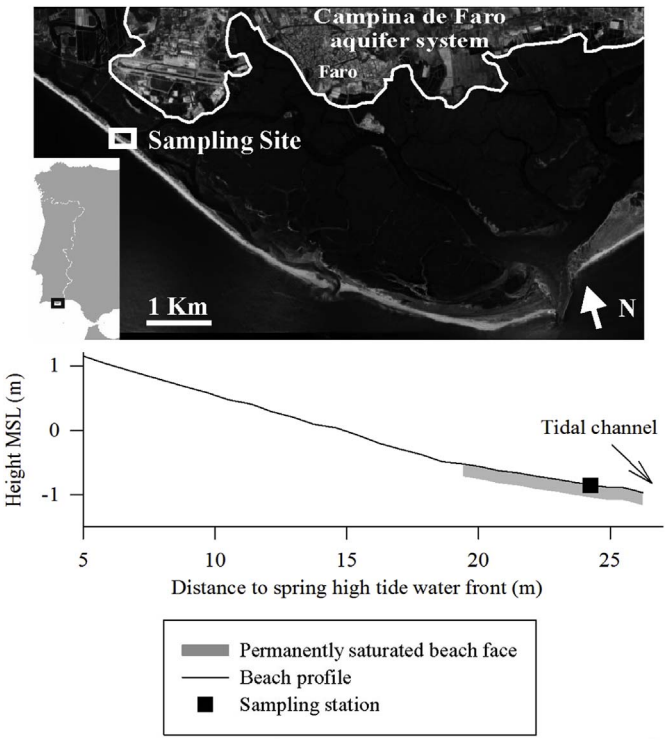

Fig. 1. Sampling site location at the inner part of Ancão peninsula, Ria Formosa coastal lagoon (SW Iberian peninsula). The location of the sampling station within the beach profile is also shown.

description of the FTR design we employed can be found in Ibánhez and Rocha (2014a). Briefly, sediment cores (40 cm length, 6.6 cm inner diameter) were collected at low tide in the lower intertidal area affected by SGD, close to the maximum discharge zone, and immediately transferred to the laboratory. There, an adapted HTH core slicer (HTH Teknik, Luleå, Sweden) was used to transfer pre-selected, undisturbed vertical sediment slices (from 2 to 12 cm depth) onto Teflon FTR cells (10 cm length, 6.6 cm inner diameter). FTR cells containing the porewater-saturated sediment were then sealed and submerged into a temperature controlled water bath in darkness. Filtered seawater (Whatman, 0.7 μm average pore size) was then pumped through the FTR cells, with attention to the original (in-situ) direction of seepage flow (deeper to shallower sediment layers, thus simulating active seepage) at a constant flow rate (from 3.7 ± 0.1 to 18.9 ± 0.3 cm h^{-1}; Table 1). Pumping of porewater at this stage progressed for 4–8 h to acclimatize the system. Longer timeframes were respected at lower velocities, such as that for all cases, a minimum of twice the porewater residence time inside the reactor passed before experiments started. This acclimatization period prior the trial runs was thought necessary to stabilize the sediment within the FTRs to the experimental temperatures and flow rates (and thus permit to stabilize the diffusive boundary layer (DBL) around sediment particles; Khalili et al., 2010), and to flush out the original porewater contained within the enclosed sediment core sections. Then, experiments were carried out with the same water flow rate as for the acclimatization phase.

The input solution was prepared from natural, filtered (Whatman, 0.7 μm average pore size), porewater collected from 40 cm depth at the seepage face with push pull mini-piezometers during low tide. This comprised essentially seawater recycled through the beach by tidal pumping, with high salinity (Table 1) and low DIN concentrations (< 10 μM; data not shown). These filtered porewater solutions were then amended with known concentrations of NO_3^- (final concentrations from 72 ± 6 to 124 ± 8 μM) and NH_4^+, both within the range of concentrations previously found at the site (Leote et al., 2008). Ammonium was added to the porewater reservoir only in experiments 7 and 8, with final concentrations ranging from 49 ± 0 to 63 ± 7 μM (Table 1). Oxygen levels were established by purging the porewater mixture with helium and/or air prior to experimental runs. The final working solution (1L for each reactor) was then placed into a sterile container, subject to constant stirring, and sealed with liquid paraffin to avoid contact with the atmosphere (Fig. 2). The final addition to the working solution was Br^- (to 1 mM final concentration), as a tracer of porewater flow and turnover timescale within the FTRs. To this end, after the acclimatization period, the FTRs were run in open mode for enough time to guarantee the internal volume of the reactor cell was flushed with the working porewater solution. Typically, this was done during a period corresponding to three times the residence time of porewater inside the reactors (Table 1). Samples were collected periodically from the outflow stream during this period, Br^- concentrations determined, and measured Br^- breakthrough curves fitted with the truncated solution of the general one dimensional advection-dispersion equation for unreactive solute transport in porous media as described by van Genuchten and Parker (1984), similarly to prior studies (e.g. Ibánhez and Rocha, 2014a, 2016). The effective dispersion coefficient (D_{ef}; the sum of the dispersive and the diffusive terms) obtained from the fitted Br^- breakthrough curves, for each reactor, was compared to that calculated as in Ibánhez and Rocha (2016). Briefly, effective diffusion in the sediment was calculated from the molecular diffusion after correction for tortuosity, calculated from the porosity by Archie's Law. Mechanical dispersion (D_{isp}) was calculated following the empirical approximation described by Bijeljic and Blunt (2006):

$$D_{isp} \sim P_e^{1.2} \quad (1)$$

where P_e is the non-dimensional hydrological Peclet number.

After renewal of the reactor's internal volume was accomplished, the outflow stream was redirected to the porewater reservoir, thus initiating the experimental run under continuous recirculation mode for a period of 50–90 h (Fig. 2). Samples were collected periodically from the porewater reservoir during the porewater recirculation, filtered through Rhizon SMS (0.1 μm pore size; Rhizosphere, The Netherlands) following the precautions suggested by Ibánhez and Rocha (2014b) and stored into sterile tubes at −20 °C until further analysis. A porewater solution identical to that used at the start of each experiment (refill solution) was used to replace the volume of sample taken from the reservoir, thus maintaining the recirculating water volume constant for the duration of the experiment. Analysis of samples was in all cases performed within a month from collection. The replenishment of the volume of working solution affects its composition, but not that of the

Table 1
List of environmental conditions characterizing each of the FTR experiments presented in this study (T-temperature; S-salinity, porewater velocity, residence time, initial O_2 and initial concentrations of NO_3^-, NH_4^+ and DOC in the porewater reservoirs). The 'Exp.' column includes the number identifying each experiment, while 'n' specifies the number of independent core slices (i.e. replicates) used for each experiment. Both calculated and modeled effective dispersion (D_{ef}) coefficients are shown for comparison. The duration of each experiment is also shown as the time elapsed since the porewater recirculation through FTR cells started (i.e. after the acclimatization period and the renewal of the internal volume of the reactors with the working solution). Uncertainty figures associated with each determination are expressed as the standard error of the estimate (SEE).

Exp.	n	Treatment	T °C	S	Duration h	$O_{2\text{-start}}$ %	Porewater Velocity (residence time) cm h^{-1} (h)	NO_3^- μM	NH_4^+ μM	DOC μmol C L^{-1}	Calculated (modeled) D_{ef} cm^2 h^{-1}
1	2	Temperature & Velocity	14.5	35.3	70	~40	18.2 ± 0.0 (0.6 ± 0.0)	89 ± 0	< 1	530	30.1 ± 0.0 (28.9 ± 1.4)
2	3	Temperature	18.5	35.3 (35)	76 ± 7	~40	18.8 ± 0.6 (0.5 ± 0.0)	87 ± 6	< 1	710 (310)	27.5 ± 0.7 (25.0 ± 9.1)
3	2	Temperature	24.5	35.4	70	~40	17.7 ± 0.6 (0.6 ± 0.0)	124 ± 8	< 1	550	24.0 ± 2.7 (23.2 ± 13.7)
4	2	Glucose added	14.5	34.2	82	~40	18.9 ± 0.3 (0.5 ± 0.0)	101 ± 6	< 1	> 2 × 10^4	31.6 ± 0.5 (26.9 ± 4.9)
5	3	Velocity	14.5	34.3	61	~40	3.7 ± 0.1 (2.7 ± 0.0)	93 ± 2	< 1	430	4.5 ± 0.1 (2.9 ± 0.3)
6	2	Velocity	14.5	34.1	64 ± 14	~40	7.3 ± 0.3 (1.4 ± 0.0)	76 ± 10	< 1	530	10.0 ± 0.7 (8.5 ± 1.9)
7	3	NH_4^+ added	14.5	34.2	70	~40	18.1 ± 0.2 (0.6 ± 0.0)	85 ± 4	49 ± 0	470	30.0 ± 0.4 (21.8 ± 8.3)
8	2	NH_4^+ & Acetylene added	14.5	34.9	63	~40	16.7 ± 1.8 (0.6 ± 0.0)	107 ± 4	63 ± 7	n.d.	27.3 ± 2.8 (24.8 ± 6.6)
9	3	O_2 saturation	18.5	35.1	90	100	18.7 ± 0.4 (0.5 ± 0.0)	72 ± 6	< 1	430	27.8 ± 0.7 (30.1 ± 4.5)

n.d. not determined.

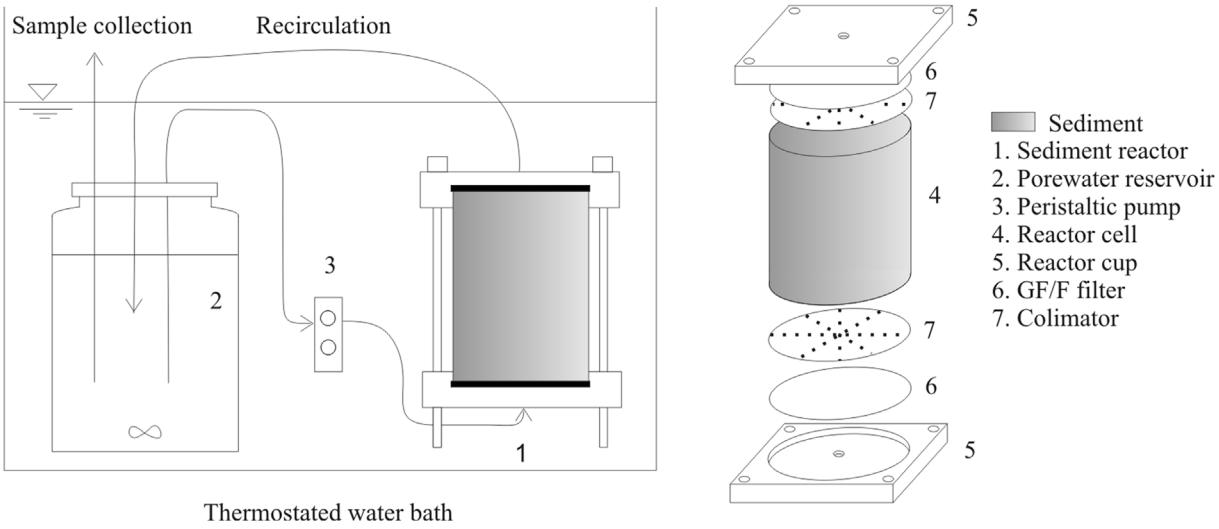

Fig. 2. Schematic view of the reactor design and the experimental set-up for the flow-through reactor experiments run under recirculation mode.

sample taken just prior to each top-up, which is only affected by previous sampling periods. Thus, it is not possible to perform an exact correction of this effect when modeling the change in porewater reservoir composition over time. To minimize this dilution effect, the composition of the porewater reservoir was corrected by the dilution effect of half the volume extracted on each sampling (20 mL). The maximum error caused by dilution of the porewater reservoir (i.e. when the difference in composition of the refilling solution and the porewater reservoir is highest) is 1.3%.

Environmental conditions at the seepage face (porewater temperature, seepage rate, oxygen concentration) that were previously measured were employed to further constrain FTR experimental conditions and to study their effects over benthic reactivity. Specifically, we tested the potential influence of:

a) Temperature: a set of three experiments (Experiments 1 to 3; Table 1) were run at different temperatures (14.5–24.5 °C) covering the range previously found on site (Leote et al., 2008; Ibánhez and Rocha, 2016). In these experiments, high porewater velocities were imposed (up to 19.1 ± 0.3 cm h^{-1}), in line with the high seepage rates measured at our site during sediment exposure (16.3 ± 2.2 to 18.6 ± 3.7 cm h^{-1} average seepage rate during active seepage; Ibánhez and Rocha, 2016);
b) organic matter availability: experiment 4 was run with glucose amendments (in excess) and results compared with those run under similar experimental settings for other factors (i.e., initial oxygen concentration, porewater velocity, temperature; Experiment 1, Table 1), to assess the possibility of organic matter being limiting of benthic inorganic N reactivity;
c) porewater velocity (interfacial advection): a set of experiments (5 and 6) was run at lower porewater velocities to those described before, in order to provide insight into the influence of interfacial advection on biogeochemical process rates and kinetics;
d) Addition of NH_4^+: NH_4^+ was added in complement to NO_3^-, to working solutions employed in experiments 7 and 8, in order to assess NH_4^+ benthic reactivity and its potential synergistic interaction with NO_3^- turnover. This assessment was complemented by information supplied by experiment 8, where the working solutions were amended with acetylene to a final concentration of 30 μM in order to block the first step of nitrification (Berg et al., 1982);
e) Initial oxygen concentration: Throughout experiments 1 to 8, the initial O_2 concentration in the porewater was adjusted to ~40% saturation by purging the porewater solution with helium and/or air. A multiparametric probe monitored the working O_2 concentration while this adjustment was performed. As an independent measure of control, the effect of O_2 saturated porewater on benthic DIN processing was carried out in Experiment 9, when the working solution was continuously aerated throughout the entire experimental run, and not protected from contact with the atmosphere with paraffin, as in all the other experimental runs.

With the exception of experiment 4, the Dissolved Organic C (DOC) content in the solution flowing through the FTRs originated from the natural in-situ composition found at the seepage face. Each experiment was run independently, in parallel, twice or thrice with the exact same input porewater for replication (Table 1). The porewater mixture for each replicate experiment was distributed through individual reservoirs, each dedicated to a different FTR. The only exception was experiment 2, which comprised replicates performed in different dates.

2.3. Ammonium adsorption isotherms

The heterogeneous equilibrium of NH_4^+ within the sediment was studied with sediment slurry incubations. The working solution was prepared from aged, oligotrophic seawater (salinity 35), amended with different NH_4^+ concentrations (from 34 to 115 μM final concentration; Fig. 3). Sediment-water slurries were prepared by mixing 10 mL of the NH_4^+ working solution with known quantities of dry sediment (2–3 g) collected at our site from 2 to 12 cm depth. Slurry incubations were performed under continuous stirring at constant temperature (15 and 25 °C). On completion, the supernatant was filtered and reserved for analysis, while the solid-phase (adsorbed) NH_4^+ was extracted from the remnant solid phase with 10 mL of 2M KCl solution for 2 h (Rosenfeld, 1979). The entire procedure was performed in duplicate. NH_4^+ partition coefficients (K*) were then calculated from the linear relationship between the NH_4^+ sorbed per g of sediment and the final NH_4^+ concentration of the incubation solutions (Rocha, 1998).

2.4. Porewater analyses

Salinity, temperature and O_2 concentration were measured with a YSI 600 multiparametric probe (Yellowspring Instruments) at the beginning of each experiment, before the working solution was sealed from atmospheric contact with paraffin oil. NO_3^-, NO_2^- and NH_4^+ concentration in the experiment samples was determined in a Lachat Quickchem 8500 Flow Injection Analysis system following standard colorimetric methods (Grasshoff et al., 1983). The method precision (MP), detection and quantification limits (DL and QL, respectively)

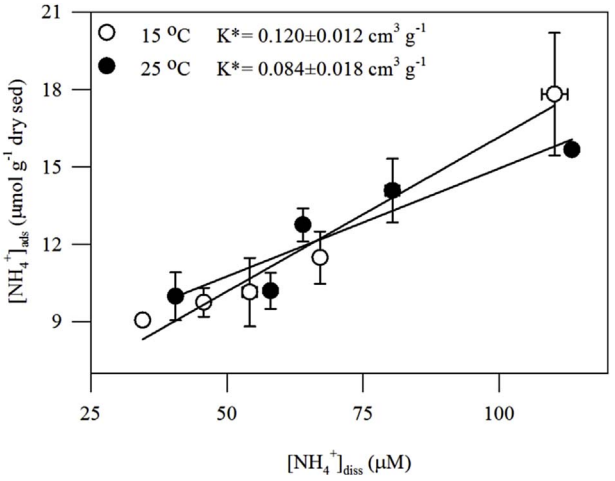

Fig. 3. Linear NH_4^+ adsorption isotherms constructed at 15 and 25 °C from the results of slurry incubations of subsurface sediment (from 2 to 12 cm depth) with aged, oligotrophic seawater (salinity 35) amended with known concentrations of NH_4^+. $[NH_4^+]_{ads}$ represents the amount of NH_4^+ adsorbed to the sediment (solid phase), while $[NH_4^+]_{diss}$ represents the equilibrium NH_4^+ concentration in the incubation solutions (solute phase). Error bars represent the SEE of the NH_4^+ concentration in both solid (vertical bars) and solute phases (horizontal bars).

were always lower than 5% (MP) and 0.5 µM (DL and QL). The concentration of Br^- was determined using a Dionex ICS-1500 Ion Chromatography system, after sample dilution with DI water to minimize interference by the Cl^- peak (MP: 6.20%, DL: 0.15 mM, QL: 0.21 mM). DOC was determined with a Vario TOC Cube elemental analyzer (MP: 3.6%, DL: 33 µmol C L^{-1}, QL: 40 µmol C L^{-1}), after removal of dissolved inorganic C by acidification (2 M HCl).

3. Approach to kinetic modeling

When conducting FTR experiments, the fluid residence time is calculated as L/v, where L is the length of the sediment column and v the advective velocity. This needs to be sufficient to induce measurable differences between the input and the output concentrations of the target analyte(s), caused by biogeochemical reactivity within the FTR (Pallud et al., 2007). As benthic reactivity in permeable sediments is regulated by porewater velocity (e.g. Boudreau et al., 2001; Rocha, 2008; Huettel et al., 2014), porewater velocities that were representative of field conditions were imposed in our FTR experiments (up to 18.9 ± 0.3 cm h^{-1}). These high advection rates might nevertheless reduce the measurement accuracy of NO_3^- reduction rates due to the consequential reduction of the residence time of the circulating fluid inside the reactor. To overcome this possible limitation of open mode experimental runs in FTRs, our experiments were run under recirculation mode.

As the volume of porewater in the reservoir was maintained at a constant level throughout each run, the solute concentrations measured with time were first transformed into total amounts by multiplication by the reservoir volume. The temporal evolution of DIN compounds was then used to study reaction kinetics for the whole sediment column section under scrutiny. To this end, reaction kinetics were described on the basis of the empirical non-linear Monod equation (Monod, 1949). NO_3^- reduction was modeled as a sequential two-step process including overall NO_3^- reduction to NO_2^- and subsequent NO_2^- reduction:

$$\frac{\partial NO_3^-}{\partial t} = -R_{max}^{NO_3^-} \frac{NO_3^-}{K_m^{NO_3^-} + NO_3^-} \quad (2)$$

$$\frac{\partial NO_2^-}{\partial t} = -R_{max}^{NO_2^-} \frac{NO_2^-}{K_m^{NO_2^-} + NO_2^-} \quad (3)$$

Because DNRA may consume both NO_3^- (with NO_2^- as an intermediary) and NO_2^- as electron acceptors, producing NH_4^+ (Lam and Kuypers, 2011), the NO_3^- reduction to NO_2^- included in equation (2) was assumed to account for the overall NO_3^- reduction, irrespective of the underlying metabolic process. The kinetics of NO_2^- reduction to NH_4^+ is then modeled with a Monod-type equation:

$$\frac{\partial NH_4^+}{\partial t} = R_{DNRA}^{NO_2^-} \frac{NO_2^-}{K_{mDNRA}^{NO_2^-} + NO_2^-} \quad (4)$$

Similarly, nitrification was initially modeled as a two-step process, including the oxidation of NH_4^+ to NO_2^- and the subsequent oxidation of NO_2^- to NO_3^-. Since NO_2^- accumulation was not observed during periods of NO_3^- build-up (i.e. assumed dominance of nitrification over NO_3^- reduction), the oxidation of NH_4^+ to NO_2^- could not be determined. Thus, the mathematical description of nitrification kinetics was simplified to include a single step reaction (oxidation of NH_4^+ to NO_3^-). Both oxygen and NH_4^+ are rate-limiting substrates for nitrification (e.g. Soetaert et al., 1996). Nevertheless, at the beginning of all experiments and when nitrification dominates, oxygen levels were sufficient to justify absence of limitation to nitrification in the reactor cell (see discussion). Furthermore, because of the absence of NH_4^+ build-up during this stage, nitrification was described in our model as progressing according to zeroth-order kinetics:

$$\frac{\partial NH_4^+}{\partial t} = -R_{ox}^{NH_4^+} \quad (5)$$

$$\frac{\partial NO_3^-}{\partial t} = R_{ox}^{NH_4^+} \quad (6)$$

Additionally, NH_4^+ sorption to sediment particles was assumed to follow first order kinetics (Fitzsimons et al., 2006):

$$\frac{\partial NH_4^+}{\partial t} = -R_{ads}(NH_{4eq}^+ - NH_{4ads}^+) \quad (7)$$

We further assumed that the heterogeneous equilibrium would be attained within 2 h (R_{ads} = 0.5 h^{-1}; Rosenfeld, 1979). NH_{4eq}^+ was calculated from the measured NH_4^+ in the porewater reservoir and the measured NH_4^+ partition coefficients (K^*) calculated from our sediment slurry incubations. K^* at the experimental temperature was obtained by linear interpolation from our adsorption isotherms, and scaled to the reactor's size according to:

$$K_{ads} = K^* \rho_s V_{reactor}(1 - \varphi)/V_{reservoir} \quad (8)$$

where ρ_s represents the sediment grain density (taken as 2.65 g L^{-1}), $V_{reactor}$ and $V_{reservoir}$ the volume of the reactor and the porewater reservoir respectively and φ the sediment porosity (from Ibánhez and Rocha, 2014a).

When acetylene blocking of nitrification was in place (Experiment 8; Table 1), observed NH_4^+ consumption was assumed to result from net assimilation by the microbial community following zeroth-order reaction kinetics:

$$\frac{\partial NH_4^+}{\partial t} = -R_{assim} \quad (9)$$

The NO_3^- concentration in the porewater reservoirs either remained unchanged or was even increased during the initial stages of the FTR experiments performed in this study. This stage was followed by a period of net NO_3^- consumption that occurred towards the end of the experimental run. In studies employing FTRs, the initial apparent inhibition of NO_3^- reduction has been described before, and accepted as a result of the time spent by the microbial community adjusting to new conditions (i.e., enzymatic induction) before NO_3^- metabolism initiates (André et al., 2011). Nevertheless, changes in the composition of the porewater reservoir over time (i.e. oxygen consumption, changes in the quantities and composition of organic matter) would also affect the net temporal and spatial balance between nitrification and NO_3^-

reduction. Hence a general inhibition/competition term was included in the model to account for the overall pattern of succession from nitrification to NO_3^- reduction over time. A general exponential decay function (I) ranging from 1 to 0 ($I = 1$ at $t = 0$) was used as an undetermined inhibition property:

$$\frac{\partial I}{\partial t} = \frac{I}{I + K_{decay}} \quad (10)$$

This was used to describe the inherent possibility of competition between nitrification and NO_3^- reduction over the experimental time frame, or simply to allow transitional inhibition affecting NO_3^- reduction (i.e. initial oxygen inhibition, initial mass transfer limitation due to the re-establishment of the stability of the DBL around sediment particles; Khalili et al., 2010) during the first stage of the FTR runs and to obtain the potential reaction kinetics (e.g. Beg and Hassan, 1987). Thus, the general expression for NO_3^- processing in the FTR experiments becomes:

$$\frac{\partial NO_3^-}{\partial t} = R_{NH_4^+ox}\left(\frac{I}{I + f_{inhibition}}\right) - R_{max}^{NO_3^-}\frac{NO_3^-}{K_m^{NO_3^-} + NO_3^-}\left(1 - \left(\frac{I}{I + f_{inhibition}}\right)\right) \quad (11)$$

Finally, DOC consumption/production rates were calculated by simple mass balance using the starting DOC concentration in the porewater reservoir and that determined throughout the experimental runs. Lastly, the modeling results are expressed in units of volume of "bulk" sediment (bs) after dividing the different parameters by the volume of the sediment within each reactor cell.

For each experiment, the resultant system of first-order ordinary differential equations was solved numerically using the lsoda method included in the ReacTran 1.3 package (Soetaert and Meysman, 2012) for R software (R Development Core Team, 2009). The fitting procedure was performed by location of the local minimum of the sum of squared residuals (SSR) between the data and the model results using the algorithm described by Nelder and Mead (1965). Due to the large number of parameters, the fitting procedure was performed sequentially (e.g. Wastney et al., 1998). First, a preliminary estimate of the rates of nitrification and NO_3^- reduction was obtained by mass balance techniques. With these preliminary figures, and assuming the absence of any inhibition of NO_3^- reduction at the end of each experiment (thus avoiding overestimation of maximum NO_3^- reduction rates), the inhibitory parameters were estimated and fixed. Finally, the fitting algorithm was used to adjust the NO_3^- and NO_2^- (and NH_4^+) distribution over time and derive the parameters describing reaction kinetics.

4. Results

4.1. Sediment and porewater characterization, flow regime within the FTRs

Taking into account our results (Fig. 2), NH_4^+ adsorption isotherms were accepted to describe linear adsorption of NH_4^+ within the range of concentrations worked with. NH_4^+ partition coefficients, obtained from the slope of the adsorption isotherms, ranged from 0.084 ± 0.018 to 0.120 ± 0.012 cm^3 gr^{-1}. NH_4^+ adsorption at our site and at the selected depth (2–12 cm) was low compared to NH_4^+ partition coefficients found in other marine sandy sediments with similar average grain size (Raaphorst and Malschaert, 1996; Rocha, 1998).

The collected porewater consisted mainly of recirculated sea water with high salinity (> 34; Table 1), in agreement with the most recent field sampling campaigns at the seepage face that identified a decrease in the freshwater contribution to SGD at the site (Ibánhez and Rocha, 2016). Natural porewater DOC content measured at the beginning of the experiments remained relatively stable, between 430 and 550 μmol C L^{-1}, during all but one of the experiments. The exception

Table 2
Results obtained from the kinetics modeling of the FTR experiments presented here. The goodness-of-fit represented by the averaged standard error (ASE) and obtained reaction rates (potential maximum nitrate and nitrite reduction, ammonium assimilation, nitrification) are shown. DOC production/consumption rates obtained by mass balance calculations are also shown. The column Exp. indicates the numbering identification of each experiment used throughout this study. bs indicates "bulk" sediment. The results obtained in the three individual reactors that showed accumulation of NH_4^+ in the porewater reservoir over time are shown separately together with the maximum potential ammonium production. Error values associated to each determination correspond to the SEE.

Exp.	ASE			NO_3^- reduction ($K_m^{NO_3^-}$) nmol cm^{-3} bs h^{-1} (nmol cm^{-3} bs)	NO_2^- reduction ($K_m^{NO_2^-}$) nmol cm^{-3} bs h^{-1} (nmol cm^{-3} bs)	Nitrification nmol cm^{-3} bs h^{-1}	Assimilation nmol cm^{-3} bs h^{-1}	DNRA ($K_{DNRA}^{NO_2^-}$) nmol cm^{-3} bs h^{-1} (nmol cm^{-3} bs)	DOC production nmol cm^{-3} bs h^{-1}
	NO_3^-	NO_2^-	NH_4^+						
1	3.2 ± 1.2	–	–	4.6 ± 0.2 (n.d.)	> > 4.6 (n.d.)	0.76 ± 0.76	–	–	−6.2 ± 1.5
2	2.9 ± 0.1	0.3 ± 0.2	–	11.5 ± 0.3 (8.3 ± 2.4)	6.1 ± 0.3 (0.4 ± 0.2)	1.04 ± 0.05	–	–	−6.4 ± 0.4
3	9.6 ± 2.3	3.2 ± 1.2	–	14.2 ± 0.2 (12.4 ± 6.4)	10.6 ± 0.4 (0.2 ± 0.0)	3.8 ± 3.8	–	–	−8.0 ± 0.5
4	3.8 ± 0.5	0.8 ± 0.8	–	5.9 ± 0.4 (0.0 ± 0.0)	> > 5.9 (n.d.)	–	–	–	–
5	0.9 ± 0.1	1.0 ± 0.2	–	4.1 ± 0.7 (1.6*)	> > 4.1 (0.3*)	0	–	–	−3.42 ± 2.0
6	1.1 ± 0.6	0.9 ± 0.5	–	6.0 ± 0.0 (7.4*)	4.9 ± 0.2 (3.3*)	0.7 ± 0.4	–	–	−4.9 ± 1.1
7	3.4 ± 0.2	0.9 ± 0.3	1.5 ± 0.0	4.0 ± 0.6 (n.d.)	3.3 ± 0.0 (n.d.)	7.5 ± 1.3	–	–	−2.4 ± 1.1
8	1.8 ± 0.7	2.0 ± 1.5	2.8 ± 0.2	5.7 ± 1.2 (6.5*)	6.2 ± 0.0 (4.2*)	0	2.0 ± 0.3	–	–
9	1.8 ± 0.4	–	–	2.3 ± 1.1 (n.d.)	> > 2.3 (n.d.)	3.0 ± 1.1	–	–	0.1 ± 1.8
DNRA									
2.C	2.6	1.8	2.2	6.2 (3.4)	0.0 (0.0)	4.6	–	8.3 (13.2)	1.7
5.C	0.9	2.1	1.4	5.72 (14.7)	0.24 (14.6)	–	–	4.1 (0.0)	1.7
7.C	2.4	1.3	4.2	6.73 (16.9)	4.4 (0.3)	3.98	–	1.2 (0.9)	1.1

*Only determined in one reactor.

was experiment 2 (Table 1), for which replicate runs were performed at different dates, and porewater used as the work solution hence originated from two different sampling events. There, the differences in the starting porewater DOC composition covered the widest range of this study, with reactors 2.A and 2.B run with porewater DOC of 710 µmol C L^{-1} while in reactor 2.C DOC was 310 µmol C L^{-1}. As DOC was not added to the natural pool (with experiment 4 where glucose was added to the porewater excepted), this variance in DOC levels corresponds to the natural variability found at the site. We exclude any major influence of potential paraffin dissolution on the changes observed in porewater composition during the experiments, firstly because of its characteristic low solubility in water (McAuliffe, 1966), and secondly because DOC measured in the porewater reservoirs decreased over time, rather than the opposite as would be expected from a constant contaminant source, in the vast majority of experiments (notable exceptions being experiment 9 run without the paraffin layer and individual replicates 2.C, 5.C and 7.C; Table 2).

The Br^- concentrations measured at reactor outlets during the acclimatization phase of the experiments (i.e. when the working porewater solutions were pumped through the sediment slices in open mode, typically during a period of three times the residence time of porewater inside the reactors) guaranteed that before recirculation mode was initiated, > 95% of the internal reactor fluid volume was renewed in all cases (e.g. Fig. 4). This ensured the absence of any significant interference of the original porewater contained within the pore structure, which could differ from core to core, on the incubation results. The breakthrough equation of van Genuchten and Parker (1984) described the measured Br^- breakthrough curves with high correlation (e.g. Fig. 4). Although the few data used in the fitting procedure would not offer a precise estimation of effective dispersion, both the modeled and calculated effective dispersion were within the same order of magnitude (Table 1), indicating that preferential flow inside the reactors was not occurring and that the matrix porosity of the sediment slices remained unchanged.

4.2. FTR experiments

Changes in NO_3^-, NO_2^- and NH_4^+ amounts over time within each porewater reservoir (when observed) are shown in Fig. 5. Two general features were common for all experiments: the first was that significant temporal changes to the DIN content were observed within the timeframe of runs. The second was that results fell into a distinct common pattern, in which a consistent temporal succession of two distinctive reactive paths affecting porewater solute levels could be inferred: porewater NO_3^- content remained unchanged or even increased during an initial period, followed by a phase of net NO_3^- removal. In some cases, the observed net NO_3^- removal led to complete depletion of porewater DIN content. NO_2^- accumulated only when net NO_3^- consumption occurred. Through the course of the experiments run in the absence of NH_4^+ addition generally no accumulation of NH_4^+ was observed. Exceptions were single runs of experiments 2, 5 and 7 (2.C, 5.C and 7.C; Fig. 5), where some NH_4^+ build up was registered. As these three single reactor runs showed a completely different reactive behavior to their equivalent replicates, the results were evaluated in a different manner (see below).

4.3. Modeling results

Our model reproduced the temporal distribution of the solutes analyzed throughout the FTR experiments with high correlation, as denoted by the low ASE. Furthermore, the model satisfactorily described the time-course change in individual DIN species (NO_3^-, NO_2^- and NH_4^+ when present) using the reactive pathways included in the primary modeling assumptions (Fig. 5). For example, it adequately described the transient NO_2^- accumulation registered when NO_2^- was considered as an intermediary compound in the two-step NO_3^- reduction model. Also, modeled results of experiments 7 and 8 convincingly predict the presence of potential nitrification within the sediment layer that was studied. Additions of NH_4^+ to the recirculating porewater during experiment 7 were satisfactorily linked to the build-up of NO_3^- through nitrification, with no NO_2^- accumulation, whereas NO_3^- remained unchanged when the first nitrification step was blocked by acetylene addition.

For NO_3^- reduction, the maximum potential reaction rates derived from the modeling procedure ranged from 2.33 ± 1.06 to 14.17 ± 0.22 nmol cm^{-3} bs h^{-1}, and likewise for nitrification, from 0 to 7.46 ± 1.32 nmol cm^{-3} bs h^{-1}. The highest potential NO_3^- reduction rates coincided with the highest temperature (24.5 °C), whereas the highest potential nitrification rate was found from the experiment run with NH_4^+ porewater amendments (experiment 7). Experiment 8 (performed under acetylene blocking of nitrification) provided useful estimates of potential microbial NH_4^+ assimilation (2.04 ± 0.00 nmol cm^{-3} bs h^{-1}). Because the half-saturation constants of NO_3^- for potential NO_3^- reduction generally found in this study where quite low, they could only be effectively determined from the results of experiments where the NO_3^- concentration in the circulating porewater attained sufficiently low values. The half-saturation constants for potential NO_3^- reduction obtained in those cases ranged from 1.6 to 16.9 nmol cm^{-3} bs (Table 2).

4.3.1. Temperature dependence of NO_3^- reduction rates

Temperature dependence of potential maximum NO_3^- reduction rates derived from modeling of the FTR experimental data is shown in Fig. 6A. Results from experiments 1, 2, 3 and 7 were included in this analysis. At the higher porewater velocity (> 16 cm h^{-1}; Table 1), reduction rates increased with increasing temperature ($p < 0.01$). Although only three different temperatures were tested in this study, the range covered allows an estimate of the sensitivity of potential maximum NO_3^- reduction rates to temperature. LnQ_{10} (Q_{10}; the relative increase in a metabolic rate when temperature increases by 10 °C) was calculated from the slope of the relation $Ln(R_{max}^{NO_3^-}/R_{max}^{NO_3^-}{}^*)$ and $(T - T^*)/10$ (Van't Hoff, 1898). $R_{max}^{NO_3^-}{}^*$ and T^* are respectively the chosen reference NO_3^- reduction rate and temperature, in this case those obtained at 18.5 °C (experiment 2). In similar fashion, the activation energy (A_e; the change in the potential energy necessary to start a metabolic process) could be calculated from the slope of an Arrhenius plot of the same results (Fig. 6B). Q_{10} calculated as described was 3.5 ± 0.2 ($p < 0.005$), whereas A_e was 0.92 ± 0.19 eV ($p < 0.005$).

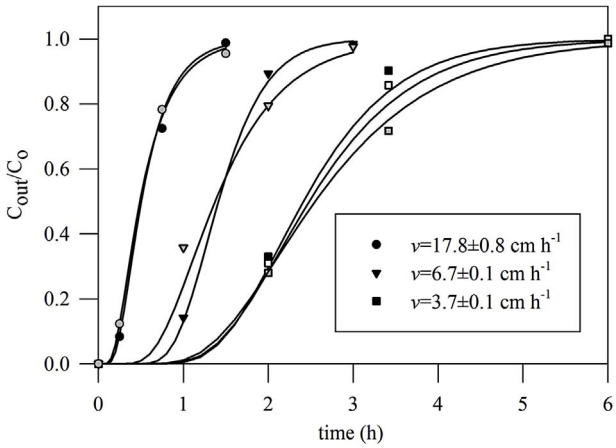

Fig. 4. Br^- breakthrough curves under different porewater velocities imposed in the FTR experiments (Experiment 1, 17.8 ± 0.8 cm h^{-1}; Experiment 6, 6.7 ± 0.1 cm h^{-1}; Experiment 5, 3.7 ± 0.1 cm h^{-1}). The proportionate change in Br^- concentration relative to initial values measured during the acclimatization phase run in open mode (C_{out}/C_0) is plotted as a function of time. Lines represent best-fit solutions of the equation described by van Genuchten and Parker (1984). Different symbol colors represent replicate runs.

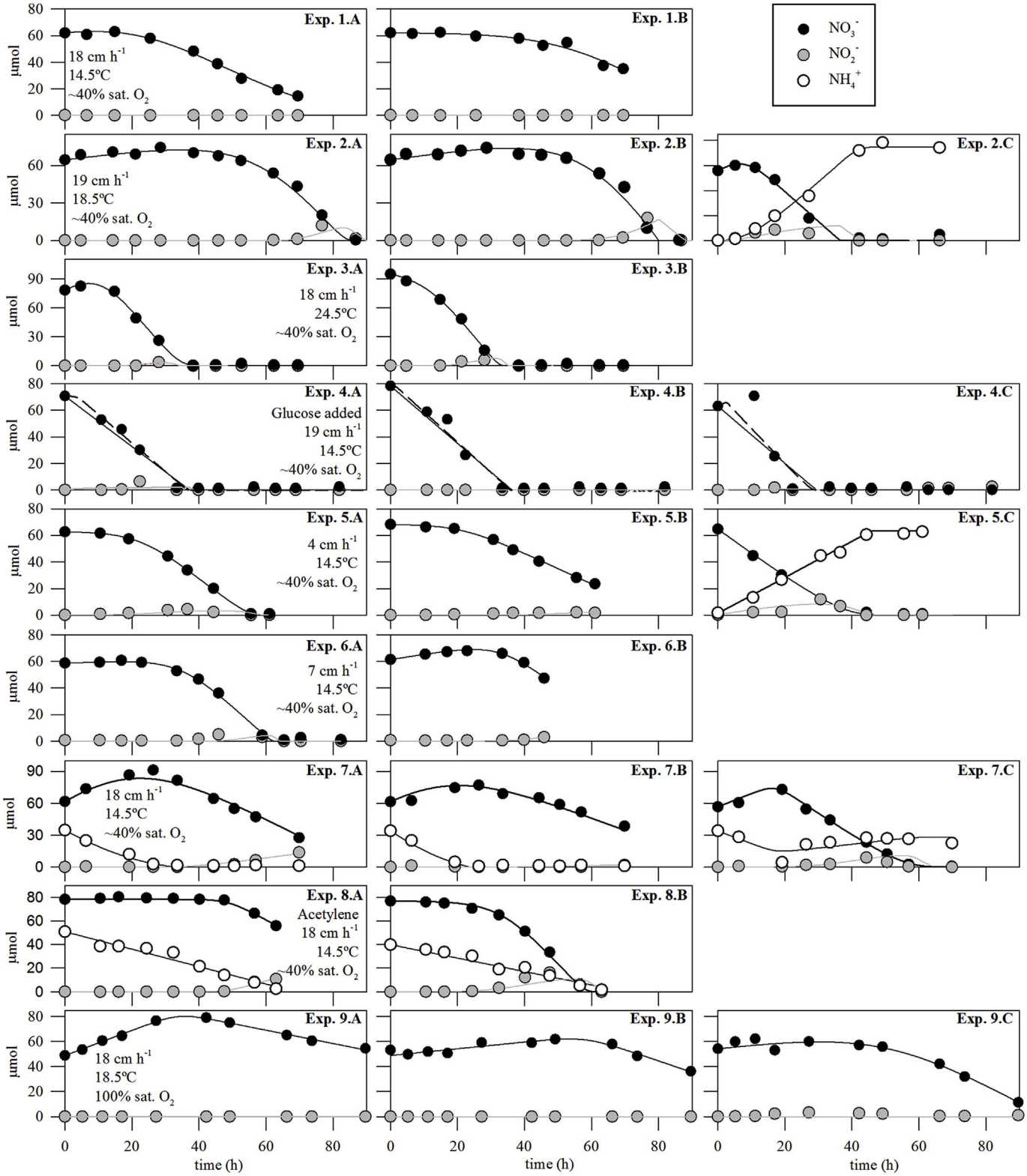

Fig. 5. Results obtained in the FTR experiments run under recirculation mode. Measured NO_3^- (black dots) and NO_2^- (grey dots) over time for each replicate used at each FTR experiment are shown together with the modeled solute temporal distribution obtained through kinetics modeling (solid lines). Measured (white dots) and modeled (solid line) NH_4^+ temporal distribution is also shown for the experiments with NH_4^+ addition to the porewater and those showing NH_4^+ accumulation over time. Relevant experimental conditions are also shown for each set of replicates.

4.3.2. Advective velocity and organic matter limitation of NO_3^- reduction

Porewater flow rate seems to affect the potential NO_3^- reduction rate (Fig. 7). At 14.5 °C, the increase in porewater velocity from experiment 5 (3.7 cm h^{-1}) to 6 (7.3 cm h^{-1}) resulted in a significant increase in maximum potential NO_3^- reduction rates, from 4.06 ± 0.67 to 6.02 ± 0.04 nmol cm^{-3} bs h^{-1} ($p < 0.05$). Further increases to the advective velocity (experiments 1 and 7; > 17 cm h^{-1}) did not extend this effect further, but resulted instead in lower

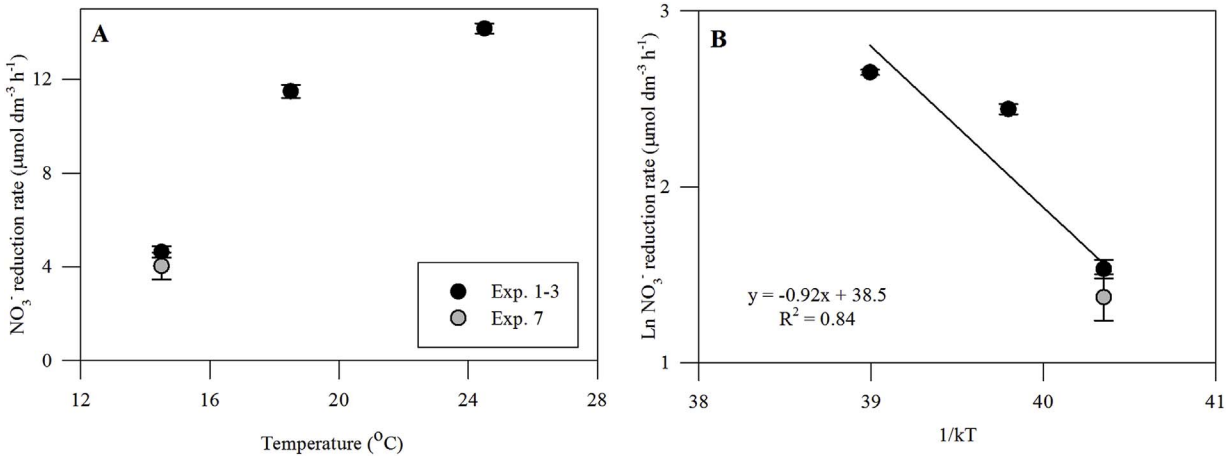

Fig. 6. A. Potential model-derived maximum NO_3^- reduction rates at different porewater temperatures (14.5 °C, 18.5 °C and 24.5 °C) for the selected sediment layer (2–12 cm depth). These correspond to experiments 1 to 3 and experiment 7. The Arrhenius plot of the modeling results is also shown (B) (k is Boltzmann's constant, 8.62×10^{-5} eV K^{-1}, and T is absolute temperature). Error bars associated to each determination correspond to the SEE.

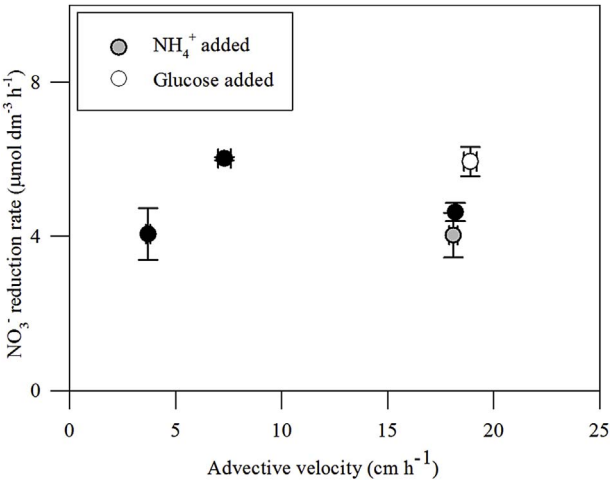

Fig. 7. Potential maximum NO_3^- reduction rates obtained through the kinetics modeling procedure under different advective regimes for the selected sediment layer (2–12 cm depth), corresponding to experiments 1 (17.8 cm h^{-1}), 6 (6.7 cm h^{-1}) and 5 (3.7 cm h^{-1}). Results from experiment 7 (18.1 cm h^{-1}), run with porewater amended with NH_4^+ (grey dot) and experiment 4 (18.9 cm h^{-1}), run with porewater amended with glucose (white dot) are also shown.

maximum NO_3^- reduction rates by comparison to experiment 6. Glucose addition to the circulating porewater (18.9 cm h^{-1}; experiment 4) stimulated maximum potential NO_3^- reduction rates (5.94 ± 0.38 nmol cm^{-3} bs h^{-1}, Fig. 7 white dots; $p < 0.05$). NO_3^- reduction rates obtained with glucose amended porewater were significantly higher than those obtained at 3.7 cm h^{-1} ($p = 0.05$), although practically identical to those obtained at 7.3 cm h^{-1}.

Addition of glucose to the porewater circulating at the highest advective velocity removed the observed inhibition/competition pattern in the remaining FTR experiments. For this experiment, the fit obtained with the more complex model including the inhibition term was compared with that obtained with a simpler model that did not include the inhibition term. A one-tailed F test was then used to test the statistical significance of the inclusion of the inhibition term on the model fit to the data (e.g. Soetaert et al., 1996). The more complex model including the inhibition terms did not significantly improve the fit of the data at the 99% confidence level ($p > 0.1$). Thus, the experiment including glucose addition was the only one suggesting no initial inhibition of NO_3^- reduction.

4.3.3. NH_4^+ production

The three individual reactors included in experiments 2, 5, and 7 showed evidence of distinctive DIN reactivity compared to the equivalent replicates (Fig. 5). The low standard error associated with the model description of the experimental data confirmed the appropriateness of the proposed mechanistic model (Table 2). In those three reactors, the kinetic model linked the observed NO_3^- reduction with NH_4^+ production, indicating NO_2^- as an intermediary.

The ratio of maximum potential NH_4^+ production to maximum potential NO_3^- reduction was high within reactors 2.C (134%) and 5.C (72%), whereas in reactor 7.C it was 18% (Table 2). Maximum NO_3^- reduction rates in reactors 5.C and 7.C were significantly higher than those observed in the equivalent replicates.

4.3.4. FTR experiment run under oxic conditions

During experiment 9, constant aeration of the porewater reservoir ensured O_2 saturation of the inflow solution throughout the experimental run. This was evaluated at the end of the experiment and, as expected, the porewater solution remained saturated in O_2 (data not shown). Despite the constant O_2 saturation of the inflowing porewater, these three reactors showed a similar pattern to those run under initial suboxic conditions: NO_3^- concentration in the porewater reservoir increased during the first hours of the experiment, followed by a significant decrease of NO_3^- concentration towards the end of the runs. Nevertheless, peak potential NO_3^- reduction rates (2.33 ± 1.06 nmol cm^{-3} bs h^{-1}) were much lower than those obtained at comparable porewater velocity and temperature (11.49 ± 0.28 nmol cm^{-3} bs h^{-1}; experiment 2; Table 1).

4.4. Sensitivity analysis of the kinetics modeling approximation

The best-fit solution of the mathematical models and the experimental data is shown in Fig. 5. A local sensitivity analysis was performed over each model fit to the data in order to evaluate the relative importance of each parameter to the solution. The normalized, scaled sensitivity analysis allowed for the assessment, at each data point, of the scaled derivative of the SSR promoted by changes on a selected model parameter (i.e. ∂SSR/∂Parameter). Fig. 8 shows the results of the sensitivity analysis for two selected examples, experiment 1 (upper panels) and 7 (lower panels). Reaction rates are those to which the NO_3^- and NO_2^- temporal distribution is more sensitive, followed by the parameters included in the inhibition/competition function. On the other hand, half-saturation constants (Monod reaction models) showed little impact over the overall fit, and as expected due to the low values obtained in the FTR experiments, only become relevant at low solute

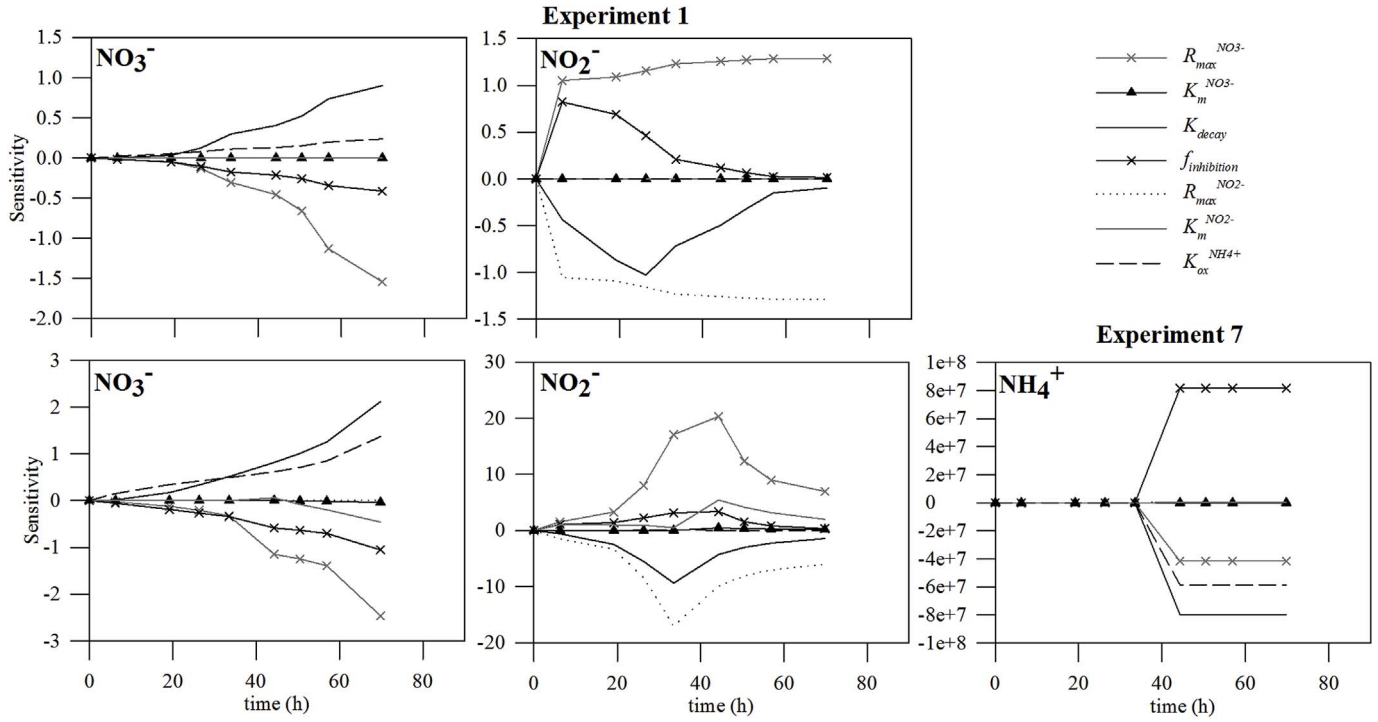

Fig. 8. Sensitivity analysis of the kinetics model used in this study. Results from experiment 1 (upper panels) and 7 (lower panels) are shown as examples. Sensitivity of the parameters included in the kinetics model over the NH_4^+ distribution in experiment 7 is shown with a logarithmic scale for clarity.

concentrations. In the experiments where NO_3^- was not completely depleted, the low impact of $K_m^{NO_3^-}$ on the modeled NO_3^- time series suggests that NO_3^- reduction at our site essentially follows zeroth-order reaction kinetics for the given NO_3^- concentrations, hence:

$$\frac{\partial NO_3^-}{\partial t} = -R_{max}^{NO_3^-} \frac{NO_3^-}{K_m^{NO_3^-} + NO_3^-} \approx -R_{max}^{NO_3^-};\ \text{when}\ NO_3^- >> K_m^{NO_3^-} \quad (12)$$

Sensitivity analysis on model fits to the NH_4^+ temporal distribution showed similar patterns to NO_3^- (Fig. 8, lower panels). Reaction rates and the inhibition function were shown to be the most sensitive parameters affecting the fit. The fit became more sensitive to the other parameters only when NH_4^+ was depleted from the porewater.

5. Discussion

5.1. Limitations in the use of FTR with water recirculation

The combination of kinetic modeling constrained by mass balance with FTR experiments run in recirculation mode allows for the determination of the potential maximum benthic reaction rates. In biogeochemical studies, FTR experiments are usually run in open mode with the composition of the inflow solution kept constant (e.g. Pallud et al., 2007; Rao et al., 2007). In open mode however, the residence time of water within the reactor cell and/or the reaction rates in place need to be sufficiently high to allow the differences in concentration between the inflow and the outflow streams to be measurable. The magnitude of the non-dimensional, first Damköhler number ($D_a = R_{max}^{NO_3^-} L/(vC_0)$; where L is the length of the reactor cell, v the porewater velocity and C_0 the initial NO_3^- concentration) is especially useful to assess whether these conditions are met, since it compares the timescales of reaction and transport in FRT experiments (e.g. Ibánhez and Rocha 2014a,b). In our experiments, D_a numbers ranged from 0.02 to 0.2 (data not shown), showing that transport dominated over reaction. For instance, in the open-mode experiments carried out by Pallud et al. (2007) D_a numbers where always much higher than 1 partially because of the low porewater velocity employed (12 ml h^{-1}). With sediment grain textures and D_a numbers (0.02) comparable to ours, Rao et al. (2007) circumvented this limitation by extending the reactor cells to 54 cm length, thus significantly increasing the residence time of water within the system (to 2.4 h). In our experiments, very high porewater velocities were imposed to match interfacial advection rates measured at the site. Combined with the relatively small length of the sediment column tested (10 cm), these high velocities resulted in characteristically short residence times (Table 1). Thus, to guarantee measurable changes in the concentrations of solutes of interest promoted by the reactivity of the sediment column within the porewater reservoir, we opted to run the FTR experiments in recirculation mode.

A further advantage of FTR experiments run in open mode is that it allows stationary state to be reached within transport and reaction time-scales, and thus the determination of reaction rates under steady state. In parallel FTR experiments run in open mode under similar conditions to those used here (porewater velocity, sediment depth) and using sediment collected during the same period (October 2010 and January 2011), stabilization of the outflow composition ensued within the timeframe of the porewater residence time inside the reactor cells (Ibánhez and Rocha, 2016). This suggests that the benthic microbial community at the study site adapts very quickly to changes in the porewater composition when interfacial flow rates remain constant, in accordance with previous observations in permeable sediments (e.g. Mills et al., 2008). Furthermore, the thickness of the DBL around sediment particles, which controls solute transport to the benthic microbial community (Khalili et al., 2010), is reduced by approximately the square root of the bulk flow velocity (Vogel, 1994). Due to the high porewater velocities imposed in our experiments, the DBL is at its lower thickness and thus, solute transport at the microscale is enhanced, explaining the fast response of the microbial community to changes in porewater composition. Thus, the fast response of the microbial community at changing porewater composition under imposed constant flow prevents the underestimation of reaction rates. Furthermore, under D_a numbers as low as those arising from the experimental conditions in this study, mass transfer of solutes can be excluded as a limiting factor for the inferred reaction rates.

Extrapolation of our FTR results to 'real-world' (i.e., field) conditions comes with some caveats however. While environmental conditions (temperature, O_2, advective velocity) imposed in these FTR experiments were based on those found on site, and care was taken to employ input solutions and undisturbed sediment columns collected from the seepage face, natural field conditions are much more dynamic than those reproduced in the laboratory. For example, tidal oscillation, which induces tidal pumping, has been identified as a main controlling factor of solute distributions and SGD rates at the Ria Formosa coastal lagoon (Rocha et al., 2009, 2015). At low tide when the beach face is exposed to the atmosphere, the seepage rates peak, but as shown in Ibánhez and Rocha (2016), the pressure balance between the internal beach aquifer and the sea surface permits surface water to infiltrate the beach aquifer through the sediment surface during high tide. This periodic surface water infiltration at high tide resupplies the sediment with dissolved and particulate organic matter, which support benthic heterotrophic processes during active seepage thru the discharge phase occurring at low tide (Ibánhez and Rocha, 2016). Furthermore, tidal pumping as described induces the periodical succession of different water masses, in terms of composition (e.g. redox potential, ionic strength, O_2) to flow through the beach aquifer, which also has a strong impact on benthic reactivity (e.g., Sun et al., 2002). This dynamism is not reproduced by our FTR experiments.

5.2. Benthic reactivity at the seepage face

Potential maximum NO_3^- reduction rates obtained by modeling of reaction kinetics in this study were in the range of 2.3 ± 1.1 to 14.2 ± 0.2 nmol cm^{-3} bs h^{-1} (Table 2). These values generally lay within the range of values found in previous FTR studies. Comparable values (3.95 nmol cm^{-3} bs h^{-1}) were found with FTR experiments run with repacked coastal carbonate sands of similar grain size and organic matter content by Santos et al. (2012). Rao et al. (2007) found significantly lower potential maximum NO_3^- reduction rates (0.02–0.11 nmol cm^{-3} bs h^{-1}) in FTR experiments with sediment of comparable grain size, but sourced from the continental shelf and containing less organic matter by weight (< 0.05%). On the other hand, Pallud et al. (2007) measured much higher potential maximum NO_3^- reduction rates (164 ± 27 nmol cm^{-3} h^{-1}) in organic-rich, fine-grained freshwater and brackish water sediments.

Half-saturation constants of NO_3^- for potential NO_3^- reduction found in our FTR experiments fall at the lower range of values previously published in denitrification studies carried out in sediments and soils (0.21–4.06 mg N L^{-1}, i.e. ~4.5–87 nmol cm^{-3} bs; Gu et al., 2007 and references therein). These values indicate a high affinity for NO_3^-, suggesting that the NO_3^- reducing microbial community at the seepage face is adapted to low NO_3^- availability. By comparison to 2005–2007, when large amounts of meteoric freshwater and groundwater-borne NO_3^- concentrations were discharged at the site (Leote et al., 2008), during this study very low seepage rates of meteoric freshwater (and hence groundwater-derived NO_3^-) to the seepage face were measured (Ibánhez and Rocha, 2016). Thus, the very low half-saturation constants of NO_3^- found here may be related to the transient hydrogeological behavior of the coastal aquifer.

Prior diagenetic modeling of benthic NO_3^- profiles covering the surface 20 cm depth horizon under steady state assumptions at our site resulted in estimates of in-situ apparent benthic NO_3^- reduction rates ranging from 0.01 to 5.2 mmol m^{-2} h^{-1} (Ibánhez et al., 2013). Integrating these over the length scale studied here (2–12 cm depth) results in net NO_3^- reduction rates of 0.05–10.6 nmol cm^{-3} bs h^{-1}. The experimental results presented here are therefore in good agreement with rates yielded by modeling of in-situ profiles, even if the NO_3^- reduction rates derived from modeling FTR reaction kinetics are potential, i.e., constitute an upper metabolic limit for the in-situ bacterial community, under similar environmental conditions. Thus, our results support the contention that high benthic biogeochemical reactivity occurs at seepage faces affected by tidal pumping and SGD. This has been shown before at our site to regulate NO_3^- loadings to the Ria Formosa lagoon through SGD (e.g. Ibánhez et al., 2011, 2013), and the conclusion could reasonably be extrapolated to other coastal and beach aquifers subject to tidal pumping (e.g. Wu et al., 2013; Santos et al., 2014).

When NH_4^+ amendments are made, the results suggest the presence of nitrification between 2 and 12 cm depth within the sediment. At high interfacial flow rates, the addition of NH_4^+ to the porewater stimulated nitrification, further suggesting that the availability of NH_4^+ in-situ may limit nitrification as previously reported (e.g. Soetaert et al., 1996). Furthermore, potential NH_4^+ assimilation estimated here resulted almost four times lower than potential nitrification measured at an equivalent porewater velocity, temperature and NH_4^+ concentration (Experiments 7 and 8, Table 2). These results suggest that NH_4^+ produced by benthic organic matter remineralization will preferentially be nitrified. This conclusion is supported further by the absence of NH_4^+ accumulation in the experiments carried out without NH_4^+ amendments (noted exceptions were 2.C, 5.C and 7.C) observed in parallel with the initial increase in NO_3^- content, suggesting that nitrification is coupled to the production of NH_4^+ via benthic organic matter remineralization in our FTR experiments.

5.3. Environmental controls over NO_3^- reduction at the seepage face

5.3.1. Temperature

The temperature dependence of potential maximum NO_3^- reduction rate was estimated to have a Q_{10} of 3.5 ± 0.2 and an A_e of 0.92 ± 0.19 eV within the range of temperatures found in-situ. The temperature dependence of potential benthic NO_3^- reduction rates found in this study is consistent with those reported in the relevant literature for similar ecosystems, in spite of the large number of microbial groups capable of using NO_3^- as the final electron acceptor in redox reactions. For instance, Laverman et al. (2006) found similar Q_{10} values (2.5–3.6) to those reported here in sediments collected from a coastal lake in The Netherlands. Rysgaard et al. (2004) reported a temperature sensitivity of 2.2 (Q_{10}) and 0.54 eV (A_e) for denitrification and 2.4 (Q_{10}) and 0.65 eV (A_e) for anammox in permanently cold sediments from Greenland. The results of this study nevertheless highlight the potential importance of short-term porewater temperature changes on the pace of NO_3^- reduction at the seepage face.

5.3.2. Seepage rate

In permeable sediments, porewater advection controls solute distribution and DBL thickness, hence regulating microbial reactivity and catabolic processes (Boudreau et al., 2001; Rocha, 2008; Khalili et al., 2010). In our FTR experiments, seepage rate (advective velocity) appears to have an important controlling role over DIN turnover rates. At the lower end of the range of tested interfacial flow velocities (3.7–7.3 cm h^{-1}; Table 1), NO_3^- reduction rate potential seems to covary with the porewater flow rate. Further increases to the flow rate (> 18 cm h^{-1}, experiments 1 and 7; Table 1) resulted in a depression of NO_3^- reduction rate potential. These results are consistent with those found by Santos et al. (2012), even if only three porewater velocities were tested in our study. In FTR experiments run with re-packed carbonate sands, the authors established that intermediate porewater velocities (from 2 to 5 cm h^{-1}) enhanced potential NO_3^- reduction, when compared to both lower and higher porewater velocities. As a result, they hypothesized that the combination of the physical structure of the sediment and the flow field at these intermediate velocities enhance the formation of highly reactive denitrifying microstructures within the sediment.

At the high-end of the porewater velocity range, the amendment of porewater with glucose in excess during experiment 4 resulted in a significant enhancement of maximum potential NO_3^- reduction rates. These results thus suggest that the magnitude of NO_3^- reduction rates

at high porewater velocities may be limited by carbon availability. This experiment was also the only one where limitation of NO_3^- reduction at the onset of test runs was not apparent (together with reactor 5.C; Table 2). Jointly, these observations also suggest that no significant microbial growth occurred during the course of the FTR experiments, and thus confirm the presence of an installed microbial capacity within the studied sediment depth horizon able to reduce NO_3^-. Indeed, the addition of glucose in excess to the porewater of FTR run under near identical conditions to experiment 4 presented here (same sediment depth from the same sampling site, equivalent temperature, porewater velocity) resulted in a significant enhancement of aerobic respiration rates, from 20.7 ± 3.8 to 34.8 ± 6.9 nmol cm^{-3} bs h^{-1} (Ibánhez and Rocha, 2016). The addition of glucose thus increases the consumption of O_2 in the porewater reservoir. At these rates, oxygen would become consumed within 9 h, explaining the apparent absence of initial NO_3^- reduction inhibition in this experiment. Even so, further studies are necessary to clarify the impact of organic matter quantity and composition over potential benthic DIN reactivity under different flow regimes in permeable sediments.

5.3.3. Oxygen

The FTR experiments reported upon in this study were initialized with circulation of porewater in suboxic conditions (~40% saturation O_2, see Table 1) with the sole exception being Experiment 9. Using the respiration rates determined at our site (Ibánhez and Rocha, 2016), oxygen consumption within the reactor cell would consume the O_2 available in the porewater reservoir within 9–27 h in experiments 1 to 8, which could explain the transition from an initial phase dominated by N oxidation (nitrification) to one where net NO_3^- consumption was observed. Although both anoxic nitrification and oxic denitrification have been described at the macroscopic level (Mortimer et al., 2004; Gao et al., 2009), the availability of O_2 is generally considered as a major environmental control over the respective reaction rates. At the scale of the microbial cell, canonic denitrification is restricted to suboxic/anoxic conditions due to electron acceptor competition and enzymatic inhibition of the denitrification pathway by O_2 (O'Connor and Hondzo, 2008). Yet, the results of experiment 9 show that at a macroscopic level, in heterogeneous environments (i.e., considering a bulk volume of sediment through which the porewater is circulating), net NO_3^- reduction is possible even if the fluid is saturated in O_2.

Jahnke (1985) explained the simultaneous O_2 and NO_3^- reduction in the presence of oxic porewater with the potential development of microenvironments within a sediment volume of interest. These would develop as a result of the patchy distribution of organic matter, leading to the presence of anoxic areas around discrete organic-rich particles driving high respiration rates in their immediate vicinity. More recently, Rao et al. (2007) showed that porewater O_2 concentrations ranging roughly from 100 to 200 μM allows anoxic microniches to form in permeable sediments, hence explaining the simultaneous occurrence of oxic respiration and anoxic denitrification in a sediment volume under study. O_2 consumption was not measured in this study. However, we performed parallel FTR experiments during the same period (October 2010 and January 2011), specifically designed to determine aerobic respiration rates at a sediment depth, porewater velocity and temperature that were comparable to the conditions imposed to the sediment studied in experiment 9 (19.2 ± 3.8 nmol O_2 cm^{-3} bs h^{-1}; 2–12 cm depth; 18.5 °C; 17.6 ± 0.1 cm h^{-1}). Results are reported in Ibánhez and Rocha (2016). Using these O_2 consumption rates as driving parameters of the 1-D steady-state, free-boundary advection-dispersion-reaction model describing the O_2 distribution in the porewater of sediments subject to active seepage described in that same study, we model the vertical distribution of O_2 within the reactor cells of experiment 9 (Fig. 9). The results show that O_2 in the porewater within the sediment column contained in the FTR cell would reach ~200 μM (190–200) at the reactors surface (near the outlet of the FTR) if the circulating solution was permanently replenished in O_2 to saturation (Fig. 8 B), but would be below ~65 μM in all other cases. Experiment 9 therefore describes the upper boundary of possible vertical porewater O_2 distributions in this sediment column, and comes within the upper limits of the O_2 concentration range proposed by Rao et al. (2007) under which anoxic microniches develop in permeable sediments. Our results thus indicate that net NO_3^- reduction is possible at our site even if the bulk sediment is apparently not anoxic.

The NO_3^- reduction rates obtained from experiment 9 were nevertheless much lower than those obtained at equivalent porewater velocity and temperature but with starting suboxic porewater circulating through the sediment. While aerobic respiration will lower down the amount of oxygen in the porewater reservoir in the FTR experiments run with initial suboxic conditions thus stopping nitrification, under permanent oxic conditions, there is no reason for aerobic, autotrophic nitrification to stop. Coupled nitrification and aerobic denitrification was shown to mask the magnitude of NO_3^- reduction rates and to promote much larger DIN removal than that corresponding to the observed NO_3^- decay in permeable sediments (Marchant et al., 2016). Thus, coupled nitrification/NO_3^- reduction could be a significant pathway of DIN loss at seepage faces.

5.4. NO_3^- reduction pathways in the FTR experiments

The potential for alternative NO_3^- reduction pathways other than canonical denitrification taking place at the seepage face limits the simple, general characterization of the final role played by the benthic community in attenuating NO_3^- pollution of surface water bodies through SGD even further. For example, the autotrophic anammox process reduces NO_2^- in tandem with the oxidation of NH_4^+, releasing N_2 gas (Thamdrup, 2012; Kraft et al., 2014). Nevertheless, anammox is inhibited at very low O_2 concentrations and the microorganisms responsible for this process have very low growth rate (e.g. Kraft et al., 2014). Due to the high O_2 concentration measured at our site during the period of this study (Ibánhez and Rocha, 2016), anammox is unlikely to have a relevant presence in our FTR experiments. However, three out of the 23 FTR experimental datasets in this study showed distinct modulation of porewater DIN fluxes compared to their respective replicates. In these cases, NH_4^+ accumulated in the porewater in parallel with the

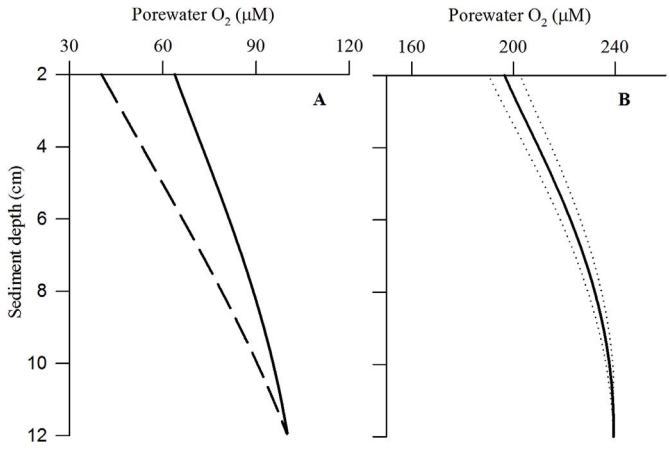

Fig. 9. A) Starting vertical distribution of porewater O_2 in reactor cells run with suboxic porewater (40% saturation) and high vertical porewater velocity (18.2 cm h^{-1}) as initial conditions (experiments 1 and 4; Table 1). The dashed line represents the model-derived vertical O_2 distribution in the porewater of experiment 4, amended with glucose. B) Starting vertical distribution of porewater O_2 in reactor cells run with an inflowing solution permanently saturated in O_2 and under high vertical porewater velocity (18.7 cm h^{-1}; experiment 9; Table 1). Porewater O_2 concentration distributions were modeled using the steady-state, advection-dispersion-reaction model described in Ibánhez and Rocha (2016). Porosity and aerobic respiration rates used were those measured at our site during the period this study was conducted (October 2010 and January 2011). Dotted lines bound the range of change in O_2 vertical distribution caused by a shift in interfacial velocities across the full range employed in all experiments.

reduction of NO_3^-. The rate of NO_3^- reduction to NH_4^+ production was in two of the three cases consistent with that characteristic of the DNRA process (Laverman et al., 2012), something also revealed at our study site when evaluating in-situ porewater DIN profiles at the seepage face (Rocha et al., 2009). Although DNRA is still poorly understood, research has suggested that it can prevail over denitrification under highly reducing conditions in organic-rich environments (Kraft et al., 2014; Hardison et al., 2015). Sulfide (and indirectly salinity as sulfate reduction increases with increased salinity) may also play an important role in regulating the relative contribution of DNRA and denitrification in N turnover by partially inhibiting the latter (Kraft et al., 2014). According to these previous studies, the conditions imposed in our experiments would not favor the occurrence of DNRA due to the very low organic matter content found at our site, along with the absence of sulfide and strong reducing conditions in the beginning of the experiments due to the pre-filtration of the porewater (and therefore heavy oxygenation of the solution). Decleyre et al. (2015) observed a high spatial variability on the relative rates and magnitudes of NO_3^- reduction pathways in estuarine sediments, where DNRA might transition from being absent to dominating NO_3^- reduction rates over length scales shorter than 2 m. Thus, spatial heterogeneity and microbial patchiness may explain the contrasting reactivity found in replicates of experiments 2, 5 and 7. Nevertheless, specific techniques such as isotopic labeling of N compounds together with isotope analysis (e.g. Kroeger and Charette, 2008) would need to be employed to confirm the presence and magnitude of alternative NO_3^- reduction pathways such as DNRA at the seepage face.

6. Conclusions

Microbial rates of nitrogen transformation at an SGD seepage face were investigated with a combination of FTR experiments and kinetic modeling. Results validated preliminary estimates of local reactivity obtained through diagenetic modeling of in-situ NO_3^- profiles collected at the seepage face. Half-saturation constants of NO_3^- for NO_3^- reduction obtained through kinetic modeling were low, suggesting high NO_3^- affinity of the NO_3^- reducing microbial community. Temperature, seepage rate and oxygen availability were identified as main environmental parameters constraining microbial processing of NO_3^- at the seepage face. Nevertheless, the results presented here illustrate how complex the benthic environment mediating NO_3^- fluxes through SGD is in terms of biogeochemistry, one where apparent aerobic NO_3^- reduction and DNRA could occur in parallel with nitrification and canonical denitrification near the sediment surface. Porewater flow, inherent of permeable sediments, controls solute distribution but also solute supply to the microbial community by determining the thickness of the DBL around the sediment particles, which in turn determines the rate of solute supply to the microbial community. The microscale heterogeneity caused by porewater flow could thus explain the simultaneous occurrence and relative importance of different reactive pathways determining the overall macroscopic benthic reactivity in mediating NO_3^- fluxes to the receiving waters. The potential sporadic presence of DNRA, suggested by some FTR replicates presented here and previous evaluation of in-situ porewater DIN profiles obtained from the seepage face (Rocha et al., 2009), together with organic matter mineralization could explain the seasonal amplification of SGD-borne NO_3^- fluxes observed at our site (Ibánhez et al., 2013).

Acknowledgments

This study was funded by the Portuguese Foundation for Science and Technology (FCT), the EU (FEDER) and the Portuguese Government through grant contract SFRH/BD/39170/2007 (Fellowship to JSPI) and project NITROLINKS - “NITROgen loading into the Ria Formosa through Coastal Groundwater Discharge (CGD) - Pathways, turnover and LINKS between land and sea in the Coastal Zone” (PTDC/MAR/70247/2006).

References

Algar, C., Vallino, J., 2014. Predicting microbial nitrate reduction pathways in coastal sediments. Aquat. Microb. Ecol. 71, 223–238.
André, L., Pauwels, H., Dictor, M.-C., et al., 2011. Experiments and numerical modelling of microbially-catalysed denitrification reactions. Chem. Geol. 287, 171–181.
Beg, S.A., Hassan, M.M., 1987. Effects of inhibitors on nitrification in a packed-bed biological flow reactor. Water Res. 21, 191–198.
Berg, P., Klemedtsson, L., Rosswall, T., 1982. Inhibitory effect of low partial pressures of acetylene on nitrification. Soil Biol. Biochem. 14, 301–303.
Bijeljic, B., Blunt, M.J., 2006. Pore-scale modeling and continuous time random walk analysis of dispersion in porous media. Water Resour. Res. 42, W01202.
Boudreau, B.P., Huettel, M., Forster, S., et al., 2001. Permeable marine sediments: overturning an old paradigm. EOS, Trans. Am. GE 82, 133–137.
Bowen, J.L., Kroeger, K.D., Tomasky, G., et al., 2007. A review of land-sea coupling by groundwater discharge of nitrogen to New England estuaries: mechanisms and effects. Appl. Geochem. 22, 175–191.
Burnett, W.C., Bokuniewicz, H., Huettel, M., et al., 2003. Groundwater and pore water inputs to the coastal zone. Biogeochemistry 66, 3–33.
Decleyre, H., Heylen, K., Van Colen, C., et al., 2015. Dissimilatory nitrogen reduction in intertidal sediments of a temperate estuary: small scale heterogeneity and novel nitrate-to-ammonium reducers. Front. Microbiol. 1124.
Erler, D.V., Santos, I.R., Zhang, Y., et al., 2014. Nitrogen transformations within a tropical subterranean estuary. Mar. Chem. 164, 38–47.
Fitzsimons, M.F., Millward, G.E., Revitt, D.M., et al., 2006. Desorption kinetics of ammonium and methylamines from estuarine sediments: consequences for the cycling of nitrogen. Mar. Chem. 101, 12–26.
Gao, H., Schreiber, F., Collins, G., et al., 2009. Aerobic denitrification in permeable Wadden Sea sediments. ISME J. 4, 417–426.
Grasshoff, K., Ehrhardt, M., Kremling, K., 1983. Methods of Seawater Analysis, second ed. Verlag Chemie.
Gu, C., Hornberger, G.M., Mills, A.L., et al., 2007. Nitrate reduction in streambed sediments: effects of flow and biogeochemical kinetics. Water Resour. Res. 43 10pp.
Hardison, A.K., Algar, C.K., Giblin, A.E., et al., 2015. Influence of organic carbon and nitrate loading on partitioning between dissimilatory nitrate reduction to ammonium (DNRA) and N2 production. Geochimica Cosmochimica Acta 164, 146–160.
Huettel, M., Berg, P., Kostka, J.E., 2014. Benthic exchange and biogeochemical cycling in Permeable Sediments. Annu. Rev. Mar. Sci. 6, 23–51.
Hwang, Dong-Woon, Lee, Y.-W., Kim, G., 2005. Large submarine groundwater discharge and benthic eutrophication in Bangdu bay on volcanic Jeju Island, Korea. Limnol. Oceanogr. 50, 1393–1403.
Ibánhez, J.S.P., Rocha, C., 2014a. Effects of recirculation of seawater enriched in inorganic nitrogen on dissolved organic carbon processing in sandy seepage face sediments. Mar. Chem. 166, 48–58.
Ibánhez, J.S.P., Rocha, C., 2014b. Porewater sampling for NH4+ with Rhizon Soil Moisture Samplers (SMS): potential artifacts induced by NH4+ sorption. Freshw. Sci. 33 (4), 1195–1203.
Ibánhez, J.S.P., Rocha, C., 2016. Oxygen transport and reactivity within a sandy seepage face in a mesotidal lagoon (Ria Formosa, Southwestern Iberia). Limnol. Oceanogr. 61, 61–77.
Ibánhez, J.S.P., Leote, C., Rocha, C., 2011. Porewater nitrate profiles in sandy sediments hosting submarine groundwater discharge described by an advection–dispersion-reaction model. Biogeochemistry 103, 159–180.
Ibánhez, J.S.P., Leote, C., Rocha, C., 2013. Seasonal enhancement of submarine groundwater discharge (SGD)-derived nitrate loading into the Ria Formosa coastal lagoon assessed by 1-D modeling of benthic NO3- profiles. Estuar. Coast. Shelf Sci. 132, 56–64.
Jahnke, R.A., 1985. Model of microenvironments in deep-sea sediments: formation and effects on porewater profiles. Limnol. Oceanogr. 30, 956–965.
Khalili, A., Liu, J., Morad, K.B., et al., 2010. Application of porous media theories in marine biological modeling. In: Vafai, K., Taylor, Francis (Eds.), Porous Media: Applications in Biological Systems and Biotechnology.
Kraft, B., Tegetmeyer, H.E., Sharma, R., et al., 2014. The environmental controls that govern the end product of bacterial nitrate respiration. Science 345, 676–679.
Kroeger, K.D., Charette, M.A., 2008. Nitrogen biogeochemistry of submarine groundwater discharge. Limnol. Oceanogr. 53, 1025–1039.
Kwon, E.Y., Kim, G., Primeau, F., et al., 2014. Global estimate of submarine groundwater discharge based on an observationally constrained radium isotope model. Geophys Res. Lett. 41 (23), 8438–8444 2014GL061574.
Lam, P., Kuypers, M.M.M., 2011. Microbial nitrogen cycling processes in oxygen minimum zones. Annu. Rev. Mar. Sci. 3, 317–345.
Laverman, A.M., Van Cappellen, P., van Rotterdam-Los, D., et al., 2006. Potential rates and pathways of microbial nitrate reduction in coastal sediments. FEMS Microbiol. Ecol. 58, 179–192.
Laverman, A.M., Pallud, C., Abell, J., et al., 2012. Comparative survey of potential nitrate and sulfate reduction rates in aquatic sediments. Geochimica Cosmochimica Acta 77, 474–488.
Leote, C., Ibánhez, J., Rocha, C., 2008. Submarine Groundwater Discharge as a nitrogen source to the Ria Formosa studied with seepage meters. Biogeochemistry 88, 185–194.
Marchant, H.K., Holtappels, M., Lavik, G., et al., 2016. Coupled

nitrification–denitrification leads to extensive N loss in subtidal permeable sediments. Limnol. Oceanogr. http://dx.doi.org/10.1002/lno.10271.
McAuliffe, C., 1966. Solubility in water of paraffin, cycloparaffin, olefin, acetylene, cycloolefin, and aromatic hydrocarbons. J. Phys. Chem. 70, 1267–1275.
Mills, H.J., Hunter, E., Humphrys, M., et al., 2008. Characterization of nitrifying, denitrifying, and overall bacterial communities in permeable marine sediments of the northeastern Gulf of Mexico. Appl. Environ. Microbiol. 74, 4440–4453.
Monod, J., 1949. The growth of bacterial cultures. Annu. Rev. Microbiol. 3, 371–394.
Moore, W.S., 1999. The subterranean estuary: a reaction zone of ground water and sea water. Mar. Chem. 65, 111–125.
Moore, W.S., 2010. The effect of submarine groundwater discharge on the ocean. Annu. Rev. Mar. Sci. 2, 59–88.
Mortimer, R.J., Harris, S.J., Krom, M.D., et al., 2004. Anoxic nitrification in marine sediments. Mar. Ecol. Prog. Ser. 276, 37–51.
Nelder, J.A., Mead, R., 1965. A simplex algorithm for function minimization. Comput. J. 7, 308–313.
O'Connor, B.L., Hondzo, M., 2008. Enhancement and inhibition of denitrification by fluid-flow and dissolved oxygen flux to stream sediments. Environ. Sci. Technol. 42, 119–125.
Pallud, C., Meile, C., Laverman, A.M., et al., 2007. The use of flow-through sediment reactors in biogeochemical kinetics: methodology and examples of applications. Mar. Chem. 106, 256–271.
R Development Core Team, 2009. R: a Language and Environment for Statistical Computing. R Foundation for Statistical Computing, Vienna, Austria.
Raaphorst, W.V., Malschaert, J.F.P., 1996. Ammonium adsorption in superficial North Sea sediments. Cont. Shelf Res. 16, 1415–1435.
Rao, A.M.F., McCarthy, M.J., Gardner, W.S., et al., 2007. Respiration and denitrification in permeable continental shelf deposits on the South Atlantic Bight: rates of carbon and nitrogen cycling from sediment column experiments. Cont. Shelf Res. 27, 1801–1819.
Rocha, C., 1998. Rhythmic ammonium regeneration and flushing in intertidal sediments of the Sado estuary. Limnol. Oceanogr. 43, 823–831.
Rocha, C., 2008. Sandy sediments as active biogeochemical reactors: compound cycling in the fast lane. Aquat. Microb. Ecol. 53, 119–127.
Rocha, C., Ibanhez, J., Leote, C., 2009. Benthic nitrate biogeochemistry affected by tidal modulation of Submarine Groundwater Discharge (SGD) through a sandy beach face, Ria Formosa, Southwestern Iberia. Mar. Chem. 115, 43–58.
Rocha, C., Wilson, J., Scholten, J., et al., 2015. Retention and fate of groundwater-borne nitrogen in a coastal bay (Kinvara Bay, Western Ireland) during summer. Biogeochemistry 125, 275–299.
Rosenfeld, J.K., 1979. Ammonium adsorption in nearshore anoxic sediments. Limnol. Oceanogr. 24, 356–364.
Rysgaard, S., Glud, R.N., Risgaard-Petersen, N., et al., 2004. Denitrification and anammox activity in arctic marine sediments. Limnol. Oceanogr. 49, 1493–1502.
Sáenz, J.P., Hopmans, E.C., Rogers, D., et al., 2012. Distribution of anaerobic ammonia-oxidizing bacteria in a subterranean estuary. Mar. Chem. 136–137, 7–13.
Santoro, A.E., 2009. Microbial nitrogen cycling at the saltwater–freshwater interface. Hydrogeol. J. 18, 187–202.
Santos, I.R., Eyre, B.D., Glud, R.N., 2012. Influence of porewater advection on denitrification in carbonate sands: evidence from repacked sediment column experiments. Geochimica Cosmochimica Acta 96, 247–258.
Santos, I.R., Bryan, K.R., Pilditch, C.A., et al., 2014. Influence of porewater exchange on nutrient dynamics in two New Zealand estuarine intertidal flats. Mar. Chem. 167, 57–70.
Soetaert, K., Meysman, F., 2012. Reactive transport in aquatic ecosystems: rapid model prototyping in the open source software R. Environ. Model. Softw. 32, 49–60.
Soetaert, K., Herman, P.M.J., Middelburg, J.J., 1996. A model of early diagenetic processes from the shelf to abyssal depths. Geochimica Cosmochimica Acta 60, 1019–1040.
Sun, M-Y i, Aller, R.C., Lee, C., et al., 2002. Effects of oxygen and redox oscillation on degradation of cell-associated lipids in surficial marine sediments. Geochimica Cosmochimica Acta 66, 2003–2012.
Swaney, D.P., Giordani, G., 2011. Proceedings of the LOICZ Workshop on biogeochemical budget methodology and applications. LOICZ Res. Stud. N0, 37.
Thamdrup, B., 2012. New pathways and processes in the global nitrogen cycle. Annu. Rev. Ecol. Evol. Syst. 43, 407–428.
van Genuchten, M.T., Parker, J.C., 1984. Boundary conditions for displacement experiments through short laboratory soil columns. Soil Sci. Soc. Am. J. 48, 703–708.
Van't Hoff, J.H., 1898. Lectures on Theoretical and Physical Chemistry. Part I. Chemical Dynamics. Edward Arnold, London.
Vogel, S., 1994. Life in Moving Fluids: the Physical Biology of Flow. Princeton University Press.
Wastney, M.E., Patterson, B.H., Linares, O.A., et al., 1998. Investigating Biological Systems Using Modeling: Strategies and Software, first ed. Academic Press, Inc., Orlando, FL, USA.
Wu, Z., Zhou, H., Zhang, S., et al., 2013. Using 222Rn to estimate submarine groundwater discharge (SGD) and the associated nutrient fluxes into Xiangshan Bay, East China Sea. Mar. Pollut. Bull. 73, 183–191.